



## Application of Brillouin thermometry to latest Pleistocene and Holocene halite from Searles Lake, California, USA



Kristian J. Olson <sup>a,\*</sup>, Emmanuel Guillerm <sup>b,c</sup>, Mark D. Peaple <sup>d</sup>, Tim K. Lowenstein <sup>a</sup>, Véronique Gardien <sup>b</sup>, Frédéric Caupin <sup>c</sup>, Sarah J. Feakins <sup>d</sup>, Jessica E. Tierney <sup>e</sup>, Justin Stroup <sup>f</sup>, Steve Lund <sup>d</sup>, David McGee <sup>g</sup>

<sup>a</sup> Department of Geological Sciences and Environmental Studies, Binghamton University, Binghamton, NY 13902-6000, USA

<sup>b</sup> Université de Lyon, UCBL, ENSL, CNRS, LGL-TPE, Villeurbanne, F-69622, France

<sup>c</sup> Institut Lumière Matière, Université Claude Bernard Lyon 1, CNRS, Université de Lyon, Villeurbanne, F-69622, France

<sup>d</sup> Department of Earth Sciences, University of Southern California, Los Angeles, CA 90089, USA

<sup>e</sup> Department of Geosciences, University of Arizona, Tucson, AZ 85721, USA

<sup>f</sup> Department of Atmospheric and Geologic Sciences, SUNY Oswego, Oswego, NY 13126, USA

<sup>g</sup> Department of Earth, Atmospheric and Planetary Sciences, Massachusetts Institute of Technology, Cambridge, MA 02139, USA

### ARTICLE INFO

#### Article history:

Received 6 March 2022

Received in revised form 17 September 2022

Accepted 11 November 2022

Available online xxxx

Editor: Y. Asmerom

#### Keywords:

Brillouin thermometry

fluid inclusions

evaporites

GDGTs

Searles Lake

### ABSTRACT

Paleoclimate records from lakes of the southwestern USA have been limited by a lack of independent paleothermometers, resulting in conflicting characterizations of millennial-scale variability in temperature and moisture. Here a novel method called Brillouin thermometry is applied to halite-bearing dry intervals of the late Pleistocene/Holocene (45–0 ka) core record of Searles Lake, California. Temperatures during muddy wetter intervals are available from branched glycerol dialkyl glycerol tetraethers (brGDGTs). Halite from the sediment-water interface records lake bottom temperatures during dry, high salinity periods. Analysis of modern saline lakes of various chemistries, depths, climate zones, and mixing regimes shows that: 1) average bottom water temperature is approximately equal to mean annual air temperature, and 2) annual range of bottom water temperature is inversely proportional to lake depth. Brillouin temperatures for eight halite intervals 30.6 ka to 8.5 ka range from  $11.8 \pm 3.6$  to  $22.4 \pm 3.2$  °C. Bottom water temperature variability indicates paleolake depths of ~10 m during halite precipitation. Temperatures from brGDGTs for mud intervals 44.7 ka to 3.6 ka range from  $13.4 \pm 2.8$  to  $23.9 \pm 3.0$  °C. Comparisons of Brillouin temperatures with predicted equilibrium temperatures of salt crystallization shed light on seasonal processes of evaporite deposition and diagenesis. The multiproxy temperature record of Searles Lake agrees with other regional records at glacial/interglacial timescales but displays a wider degree of millennial-scale variability, with temperatures during the last glacial ranging from 8.3 °C below modern mean annual temperatures to 3.8 °C above.

© 2022 Elsevier B.V. All rights reserved.

### 1. Introduction

Closed basin lake deposits are important archives of continental paleoclimates (Smoot and Lowenstein, 1991). They accumulate sedimentological, biological, and hydrological data from regional-to-intrabasinal spatial scales and millennial-to-diurnal temporal scales (Feakins et al., 2019; Lowenstein et al., 1999; Olson and Lowenstein, 2021; Sirota et al., 2017). The sensitivity of closed basin lakes to changes in inflow/evaporation makes them particularly useful for reconstructing regional responses to climate vari-

ability, especially when predicting future drought in water stressed regions such as the southwestern USA (Cook et al., 2021; Pierce et al., 2013; Seager et al., 2007, 2009).

Multiple studies of closed basin lakes in the southwestern USA provided detailed records of millennial-scale hydrologic variability but were limited by a lack of available independent temperature proxies, instead characterizing moisture-temperature relationships by temporal correlations to North Atlantic stadial/interstadial variability (Bacon et al., 2020; Benson, 1999; Benson et al., 2003; Lin et al., 1998; Lund et al., 2021; Phillips et al., 1994; Reheis et al., 2015). But these studies differed over whether warm interstadials were wet or dry (and vice versa), which led to differing interpretations of the mechanisms driving regional paleoclimate variability. Recent advances in lacustrine paleothermometry include clumped

\* Corresponding author.

E-mail address: [kolson2@binghamton.edu](mailto:kolson2@binghamton.edu) (K.J. Olson).

isotope thermometry from carbonates (e.g., Santi et al., 2020), coupled glacier-lake models (Quirk et al., 2018), and sensitivity scaling of proxy compilations (Ibarra et al., 2018). Here we offer a new paleotemperature technique suitable for halite formed in hypersaline lakes.

Subsurface deposits at Searles Lake, California USA, are characterized by interbedded muds and salts which document fluctuations in lake level of ~100 to 200 m and water volumes by 30–90 km<sup>3</sup> (Smith, 2009). Wet periods (net inflow > net evaporation) are recorded by mud deposition and salts form during dry periods (net evaporation > net inflow). Halite is the most soluble mineral in the Searles Lake deposit (Olson and Lowenstein, 2021) and thus marks periods when lake water was most concentrated (i.e., periods of hyperaridity). Here, two independent temperature proxies are used to reconstruct temperatures during dry (salt) periods and wet (mud) periods and therefore clarify the relationship between temperature and moisture within a single depositional setting, without relying on chronologic correlations to North Atlantic events or inferring temperature from other proxy records.

First, a new temperature proxy called Brillouin thermometry (El Mekki-Azouzi et al., 2015) is applied to fluid inclusions in halite from Searles Lake. As halite precipitates, slight imperfections in the propagating crystal produce small voids which entrap microdroplets of brine called fluid inclusions. Such fluid inclusions are primary, discrete, rapidly formed, and exquisitely preserved aliquots of the brine from which the halite crystal precipitated. These fluid inclusions preserve the physical characteristics of the paleobrine which can be used to determine the temperature of the brine at the time of fluid entrapment. The first method developed to use halite inclusions as a paleotemperature proxy, referred to as microthermometry, required nucleating a vapor bubble within the fluid inclusion and then observing the temperature at which the vapor phase homogenized into the liquid phase, called the homogenization temperature (Roberts and Spencer, 1995). Although theoretically sound, the method of homogenization temperatures suffered from analytical problems and failures in reproducibility (e.g., Guillerm et al., 2020; Lowenstein et al., 1998). However, the applicability of halite fluid inclusions as accurate paleothermometers has recently been rejuvenated using Brillouin spectroscopy (Guillerm et al., 2020). This new technique uses the same theoretical principles governing homogenization methods, but without the analytical limitations. Both methods are described in the Supplementary Material.

Next, depositional temperatures from interlayered mud units are derived from bacteria-derived branched glycerol dialkyl glycerol tetraethers (brGDGTs) whose relative abundance of specific brGDGTs has been demonstrated to be influenced by temperature and this is reflected in the methylation index of tetraethers (MBT'<sub>5Me</sub>) (De Jonge et al., 2014). Global calibrations of lake core top MBT'<sub>5Me</sub> to mean temperature of months above freezing ( $r^2 = 0.83$ , RMSE = 2.9 °C) (Martínez-Sosa et al., 2021) are applied to the brGDGT record from Searles Lake (Peaple et al., 2022). MBT'<sub>5Me</sub> in hypersaline and alkaline lakes fall off the global calibration temperatures (Martínez-Sosa et al., 2021; Wang et al., 2021), but Peaple et al. (2022) found no correlation with downcore salinity estimates for Searles Lake, while finding plausible temperatures and temperature shifts across key transitions in the mud deposits. Here, we compare Brillouin and brGDGT temperature estimates from salt and mud in a core (SLAPP-SRLS17-1A) taken from Searles Lake. The Brillouin/brGDGT temperature record is then compared with Searles Lake paleobrine temperatures predicted from evaporite mineral equilibria in the same sediment archive (Olson and Lowenstein, 2021). This multiproxy comparison reveals the sensitivity of evaporites to temperature-driven alteration and provides insights on the relationship between salt deposition and seasonal temperature variability in perennial saline lakes.

### 1.1. Searles Lake evolution & history

Pleistocene–Holocene Searles Lake, California, was a saline-alkaline lake fed by the ancestral Owens River (Fig. 1A). The modern Owens River is primarily fed by runoff along the eastern flank of the Sierra Nevada and since 1913 has been diverted by the Los Angeles Aqueduct, upstream of the now dry Owens Lake (Fig. 1A) (Pretti and Stewart, 2002). During pluvial conditions, the Owens River was the link in a chain of five lakes formed by successive downstream spillover: Owens Lake spilled into China Lake which, in turn, spilled into Searles Lake. At high lake levels, Searles Lake coalesced with China Lake and spilled into Panamint Lake. Lastly, when Panamint Lake overflowed, it spilled into Lake Manly in Death Valley (Gale, 1914; Smith, 1979; Reheis et al., 2014). Searles Lake likely overflowed during Marine Isotope Stages 2 and 6 but was otherwise the terminus for the Owens River throughout much of the Late Pleistocene (Smith, 2009). Today Searles Lake is a dry saline pan (Fig. 1B).

Fluctuations in inflow and evaporation rates during the Pleistocene and Holocene are loosely characterized by the alternating deposits of salts and muds in Searles Lake (Fig. 1C) (Smith, 2009). Hydrothermal spring flow from Long Valley Caldera (Fig. 1A) in the upper Owens River catchment today contributes 1/3 of the total solutes to the Owens River and accounts for much of the river's bulk chlorinity and alkalinity (Pretti and Stewart, 2002). Evaporation of Owens River water produces a complex suite of chemical sediments including carbonates, sulfates, borates, silicates, and chlorides – in the form of ~25 different minerals (Smith, 1979; Olson and Lowenstein, 2021).

Brine evolution at Searles Lake, driven by evaporation, is characterized by the following mineral sequence (Fig. 2, Olson and Lowenstein, 2021). First, calcite/aragonite [CaCO<sub>3</sub>] and dolomite [CaMgCO<sub>3</sub>] precipitate and are deposited along with clastic silt and clay as laminated mud on the lake floor. Upon further evaporative concentration, calcite/aragonite are replaced by displacive crystals of gaylussite [Na<sub>2</sub>Ca(CO<sub>3</sub>)<sub>2</sub> · 5H<sub>2</sub>O] or pirssonite [Na<sub>2</sub>Ca(CO<sub>3</sub>)<sub>2</sub> · 2H<sub>2</sub>O]. Further evaporation results in precipitation of Na-carbonates (e.g., trona [Na<sub>2</sub>CO<sub>3</sub> · NaHCO<sub>3</sub> · 2H<sub>2</sub>O] or natron [Na<sub>2</sub>CO<sub>3</sub> · 10H<sub>2</sub>O]) and Na-sulfates (e.g., burkeite [Na<sub>6</sub>(CO<sub>3</sub>)(SO<sub>4</sub>)<sub>2</sub>] or mirabilite [Na<sub>2</sub>SO<sub>4</sub> · 10H<sub>2</sub>O]). These sodium-bearing minerals form at the air-water interface or in the water column and are deposited as “cumulates” on the lake bottom after settling through the water column. The last mineral to form is halite [NaCl], which precipitates on the lake floor as “bottom growth”.

Olson and Lowenstein (2021) found that the predominant saline mineral sequence in the Lower Salt and Upper Salt at Searles Lake is trona → burkeite → halite, which indicates brine temperatures between 20–29 °C during evaporite precipitation. However, these temperature estimates only consider the evaporite record from a thermodynamic perspective, and temperatures for sequences of evaporites which likely reflect hundreds of years of deposition. This temperature estimate also does not take into account the conditions under which saline minerals form in mud units, such as gaylussite and pirssonite (Olson and Lowenstein, 2021). Furthermore, the estimated 20–29 °C range during deposition of the Lower Salt and Upper Salt is at the upper end of the 8.2–32.8 °C range of mean monthly temperatures for modern Searles Valley (NOAA National Climatic Data Center). Thermodynamic models show that the solubilities of Na-carbonates and Na-sulfates are temperature-sensitive, especially the low temperature salts natron and mirabilite, both of which are absent in the subsurface of Searles Lake.

Here, the Brillouin method is tested as a novel paleothermometer for times of halite precipitation and brGDGTs are used to independently constrain temperatures during mud deposition. Comparisons between the Brillouin/brGDGT temperatures and the

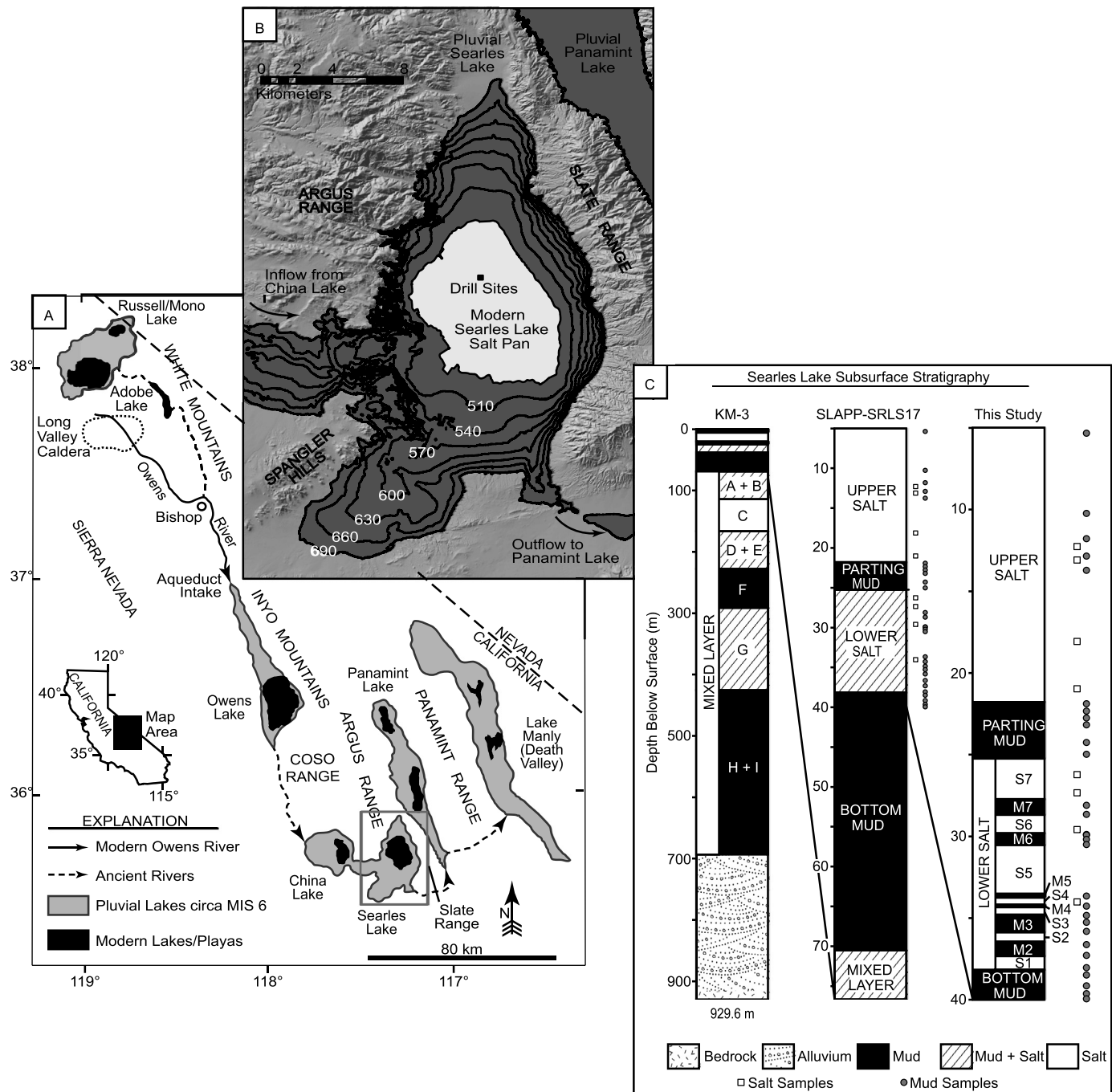


**Fig. 1.** Study region and core records. (A) Regional map showing modern rivers and lakes/playas and the maximum extent of their pluvial counterparts during Marine Isotope Stage (MIS) 6. LVC = Long Valley Caldera. (B) Map of Searles Valley showing pluvial lake elevations and extent of modern salt pan. (C) Searles Lake subsurface stratigraphy from core KM-3 and nearby core SLAPP-SRLS17-1A/B. Lower Salt divided into salts (S1-7) and muds (M2-7). Modified from Smith (2009); Olson and Lowenstein (2021).

thermodynamic-based evaporite facies are then used to obtain a lake temperature record that covers both wet (mud) high lake levels and dry (salt) low lake levels.

## 2. Materials and methods

### 2.1. Searles Lake sediment core

Sonic drilling was used to recover sediment cores from Searles Lake in January 2017 (Fig. 1B, C). Core SLAPP-SRLS17-1A (35.73715, -117.33029), drilled to 76.7 meters below surface (mbs), records ~200 kyr of lake deposition (Bischoff et al., 1985). A second core,

SLAPP-SRLS17-1B (35.73715, -117.33033), was drilled from 21.7 to 38.8 mbs to ensure complete recovery of the Lower Salt. Core description, sampling, and photography were performed in 2017 at the Continental Scientific Drilling (CSD) Facility, University of Minnesota. Chronostratigraphy was established using U/Th disequilibrium dating and BACON age-modeling (Fig. S7) (Stroup et al., 2022). Thin section microscopy was used to identify eight halite layers exhibiting bottom-growth textures, which indicates that 1) the halite is primary and 2) the primary fluid inclusions formed at the sediment-water interface at the bottom of the lake and therefore record lake floor temperatures. Halite crystals were removed

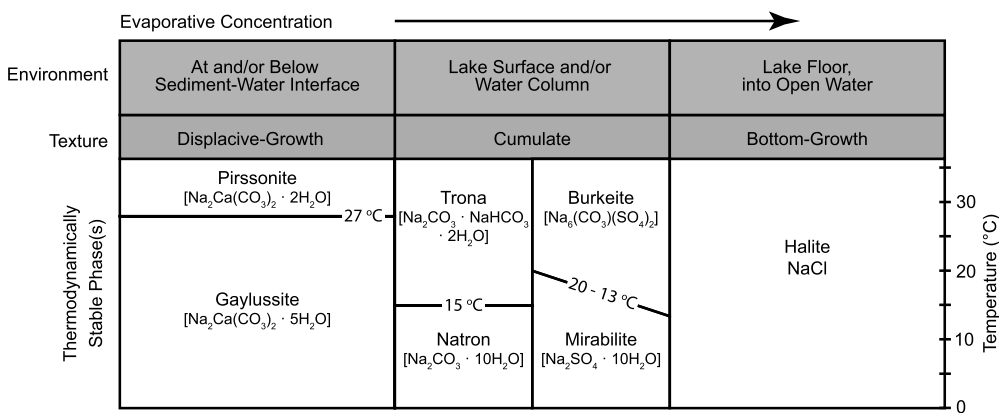


**Fig. 2.** Environment, texture, and Searles Lake evaporite minerals as a function of brine concentration and temperature (modified from Olson and Lowenstein, 2021).

from a ~2 cm thick interval of each layer and then cleaved into ~0.5 cm<sup>2</sup> fragments for fluid inclusion analysis.

## 2.2. Brillouin thermometry

Brillouin thermometry was performed at Université Claude Bernard Lyon 1, Lyon, France. The experimental apparatus is illustrated in Fig. S2 and the method briefly outlined here and the Supplementary Material. For a comprehensive overview of the theory and methodology of Brillouin thermometry, see El Mekki-Azouzi et al. (2015); Guillerm (2019); Brall et al. (2022), and Guillerm et al. (2020). Halite samples were placed in a temperature-controlled heating-cooling stage (Linkam, Tadworth, UK, THMS600) and observed with a microscope/camera (Zeiss Axioscope) to select and document fluid inclusions which met the size, depth, and isolation criteria outlined by Guillerm et al. (2020). A 4 W, 532 nm longitudinal monomode laser beam was generated (Coherent, Verdi V6) and split into a reference beam which bypassed the experimental setup, and an experiment beam. The experiment beam, dimmed to 54 mW, entered the microscope, passed through the objective (Mitutoyo PlanApo, 100x magnification), and focused to a 1 μm spot size on a fluid inclusion. The backscattered light was analyzed with a six-pass tandem Fabry-Pérot interferometer (JRS Scientific, Mettmenstetten, Swiss, TFP-1) to measure the frequency shift of the inelastically scattered light with respect to the reference laser beam. The Brillouin frequency shift ( $\Delta f_B$ ) was then used to derive the acoustic velocity of the fluid inclusion and plotted as a function of the temperature of the experiment (Fig. A-1D).

Brillouin thermometry was performed on four to nineteen fluid inclusions per ~0.5 cm<sup>2</sup> crystal, and two to three crystals per ~2 cm thick halite layer. The acoustic velocity of each fluid inclusion was measured at four temperatures (e.g., 5, 13, 21, 29 °C). Once quasi-isochoric measurements were completed, the sample was heated to 130 °C and then cooled to room temperature in order to cause an irreversible increase in the volume of the inclusions, and thus nucleate a vapor bubble in the fluid inclusions. The acoustic velocity of each, now biphasic, fluid inclusion was measured at four temperatures, which defines the curve along liquid-vapor equilibrium (LVE). A parabolic best-fit of the two sets of four data-points was used to define the isochore and LVE, respectively.  $T_x$  is defined as the point where the two curves intersect (Fig. A-1D).

$T_x$  was determined for each individual fluid inclusion measured with an analytic error of ~2 °C (Supplementary Material). The tiny size (3–23 μm) of the fluid inclusions relative to halite precipitation rate (~ cm/yr scale) ensures that each fluid inclusion records a temporally precise 'snapshot' of brine temperature. The average  $T_x$  for a whole crystal is obtained by calculating the average of the individual fluid inclusion  $T_x$  population with standard error calculated using a Student's t-distribution.  $T_x$  for a stratigraphic

layer was calculated as a weighted average from the mean and SD of the crystals within the layer.  $T_x$  is therefore considered at three different spatiotemporal scales: the fluid inclusion scale, the halite crystal scale, and the halite layer scale. The latter provides the best representative average bottom water temperature, whereas the minimum-maximum difference between the halite crystals within the stratigraphic layer ( $T_x$  range) provides insight into the shorter, probably seasonal, temperature variations (Brall et al., 2022).

## 2.3. GDGT analyses

Ground, dried sediments (~20 g) were extracted using a Dionex Accelerated Solvent Extraction system at the University of Southern California with 9:1 dichloromethane (DCM):methanol (MeOH) at 100 °C and 1500 psi to yield the total lipid extract (TLE). The TLEs were then separated into neutral and acid fractions using columns packed with NH<sub>2</sub> coated silica gel. Neutral fractions were eluted using 2:1 DCM:isopropanol. The neutral polar fraction was dissolved in hexane:isopropanol (99:1) and filtered through a 0.45 μm PTFE filter prior to analysis by Agilent 1260 High-Performance Liquid Chromatography (HPLC) coupled to an Agilent 6120 mass spectrometer at the University of Arizona. Separation of the brGDGTs was achieved using two BEH HILIC silica columns (2.1 mm × 150 mm, 1.7 μm; Waters) following the methods of Hopmans et al. (2016). The relative methylation of the 5' isomers of the brGDGTs is expressed as the MBT'<sub>5Me</sub> index (De Jonge et al., 2014).

$$\text{MBT}'_{5\text{Me}} = (\text{Ia} + \text{Ib} + \text{Ic}) / (\text{Ia} + \text{Ib} + \text{Ic} + \text{IIa} + \text{IIb} + \text{IIc} + \text{IIIa}) \quad (1)$$

Duplicate analyses as well as analyses of an internal laboratory standard throughout the runs yielded an error of 0.009 MBT'<sub>5Me</sub> units ( $1\sigma$ ). A 200 kyr record of brGDGT temperatures for Searles Lake is reported by Peaple et al. (2022). In that study, Searles Lake brGDGTs distributions are compared with the distribution of brGDGTs from global lake and soil datasets and they find that a lake calibration is most appropriate. We therefore convert MBT'<sub>5Me</sub> into mean temperature of Months Above Freezing (MAF) using a Bayesian global lake calibration BayMBT<sub>0</sub> (Martínez-Sosa et al., 2021) with reported calibration RMSE of 2.9 °C ( $n = 65$ ,  $R^2 = 0.82$ ).

## 2.4. Modern analogs

Meaningful interpretation of Pleistocene Searles Lake bottom water temperatures requires knowledge of the relationship between the air, surface water, and bottom water temperatures of modern saline lakes. These relationships are first established for

**Table 1**  
Summary of Brillouin thermometry data for Searles Lake, California.

Stratigraphic Unit	Sample ID	Depth <sup>*</sup> (cmbs)	Age <sup>†</sup> (kya)	Population <sup>§</sup>	n	SD	Bottom Water Temperature (°C)		MSWD <sup>**</sup>	Maximum <sup>††</sup> Lake Depth(m)
							Mean	Range <sup>#</sup>		
Upper Salt	1A-6V 68-70 cm	12.27	8.5 ± 0.9	Crystal 1	8	2.2	21.6 ± 0.9			
				Crystal 2	8	0.9	21.1 ± 0.4			
				Crystal 3	5	1.2	26.8 ± 0.7			
	1A-7V 67-69 cm	13.09	9.0 ± 0.9	Average	3	2.3	22.4 ± 3.2	5.7 ± 0.8	30	10.4–19.0
				Crystal 1	4	1.8	17.1 ± 1.2			
				Crystal 2	6	1.8	22.1 ± 0.9			
	1A-10V 108-111 cm	18.08	12.1 ± 0.8	Crystal 3	9	2.2	18.3 ± 0.8			
				Average	3	2	19.4 ± 2.6	5.0 ± 1.5	7.5	10.6–19.4
				Crystal 1	8	1.9	23.9 ± 0.8			
	1B-7V 85-87 cm	20.97	14.0 ± 0.4	Crystal 2	5	2.5	18.3 ± 1.5			
				Crystal 3	8	2	19.8 ± 0.8			
				Average	3	2.2	21.4 ± 2.9	5.6 ± 1.7	11	10.4–19.4
Lower Salt	S7 1B-10V 104-106 cm	26.22	23.1 ± 0.5	Crystal 1	10	1.9	22.6 ± 0.7			
				Crystal 2	4	1.5	22.7 ± 1.1			
				Crystal 3	7	2.3	21.7 ± 1.0			
	1A-16V 131-133 cm	27.33	23.8 ± 0.5	Average	3	0.4	22.4 ± 0.5	1.0 ± 1.5	0.31	NA
				Crystal 1	17	3.2	15.9 ± 0.8			
				Crystal 2	5	1.5	10.9 ± 0.8			
	S6 1B-12V 139-141 cm	29.58	26.1 ± 0.9	Crystal 3	4	3.9	8.6 ± 2.7			
				Average	3	2.6	13.2 ± 3.6	7.3 ± 2.8	18	10.1–18.0
				Crystal 1	5	2.3	18.0 ± 1.3			
	S4 1B-16V 25-27 cm	34.01	30.6 ± 1.0	Crystal 2	5	4.8	12.9 ± 2.7			
				Average	2	2	17.0 ± 3.6	5.1 ± 3.0	2.9	10.5–19.4
				Crystal 1	19	2.7	18.5 ± 0.7			
				Crystal 2	6	2.6	21.1 ± 1.3			
				Average	2	1.1	19.1 ± 1.8	2.6 ± 1.5	3.1	11.1–20.9
				Crystal 1	9	2.9	10.4 ± 1.1			
				Crystal 2	9	2.5	15.3 ± 1.0			
				Crystal 3	9	3.2	8.6 ± 1.2			
				Average	3	2.9	11.8 ± 3.6	6.7 ± 1.6	11	10.2–18.4

\* cmbs = composite meters below surface.

† BACON age model based on U/Th geochronology,  $2\sigma$  uncertainties. (Stroup et al., 2022).

§ For Crystals, uncertainties given as standard error using a Student's t-distribution. Layer Averages are computed from the mean and SD of the two or three Crystals. Estimated uncertainty (SD) is biased weighted, temperature is weighted mean, and uncertainty ( $\pm$ ) is unbiased weighted SD.

# BWT Range = Maximum Crystal temperature - Minimum Crystal temperature  $\pm 1\sigma$ .

\*\* Mean square weighted deviation.

†† Computed from BWT Range using equations from Fig. 5E (lower estimate) and Fig. 6A (upper estimate).

Great Salt Lake, Utah, using the Great Salt Lake chemical database which is maintained by the Utah Geologic Survey and contains high-resolution lake temperature data from 1966 to 2014 (Rupke and McDonald, 2012). Great Salt Lake is an appropriate analog for reconstructing temperatures at Searles Lake due to the large seasonal variability in temperature as well as its periodic supersaturation with respect to mirabilite and halite. Nonetheless, saline lakes are unique with respect to chemistry, stratification, hypsometry, volume, surface area, and geography. As such, any prudent application of a modern lake as an analog for an ancient system requires multiple analogs, where available, to increase confidence that an observed behavior is characteristic of saline systems in general. For this reason, additional data from nine non-tropical saline lakes of various depths and salinities are used to confirm the relationships observed in Great Salt Lake (Supplementary Material).

### 3. Results

Brillouin thermometry is applied to four layers from the Upper Salt (15.6–0 ka) and four layers from the Lower Salt (38.5–22.6 ka). All the halite samples are separated by muds (Lower Salt) or non-halite evaporites (Upper Salt), except for two samples from the S7 unit of the Lower Salt. The fluid inclusions analyzed in multiple crystals from each layer were used to determine a bottom water temperature for each crystal, and the maximum, minimum and mean bottom water temperature for each layer (Table 1). For the Upper Salt, mean bottom water temperatures vary from  $19.4 \pm 2.6$  to  $22.4 \pm 3.2$  °C with ranges of 3.0 to 7.8 °C. The Lower Salt yields a mean of  $11.8 \pm 3.6$  to  $19.1 \pm 1.8$  °C and range of 4.6 to 10.8 °C.

Estimating depositional rates of evaporites is difficult given 1) the bimodal crystallization rates for cumulates and bottom growth and 2) the sensitivity of crystallization rates to changes in temperature, evaporation, and ionic composition. The age model indicates accumulation of 0.16 cm/yr for the S7 halite unit (Stroup et al., 2022), or 13 yrs for 2 cm. However, halite deposition rates are typically much faster in modern systems (e.g., Dead Sea, 10 cm/yr, Lensky et al., 2005), indicating that alternating muds are slowing the apparent accumulation rate in S7 and 2 cm of halite crystals could represent  $<1$  yr.

Unlike Brillouin thermometry on selected crystals in the halite layers, brGDGT thermometry can be continuously applied across the mud units (including the Parting Mud, Bottom Mud, and M6) to yield a timeseries from which variability can be assessed. BrGDGT temperature estimates range from  $13.4 \pm 2.8$  °C to  $23.9 \pm 3.0$  °C, with an average of  $18.7 \pm 2.8$  °C from 45–0 ka (Table 2). The average depositional rate for the Parting Mud is 0.05 cm/yr (Stroup et al., 2022), so brGDGTs extracted from 2 cm samples integrate  $\sim 40$  yrs.

### 4. Discussion

#### 4.1. From temperature to lake depth

To ascertain the climatic significance of the Brillouin thermometric data from Searles Lake halite, a relationship must be established between the temperatures on the lake floor where halite crystals grow and mean annual or seasonal air temperatures. Additionally, the variable(s) controlling annual fluctuations in bot-

tom water temperature must be determined, as well as the relationship between the average temperatures and the temperature ranges.

The thermal structure, mixing, and bottom water temperatures of freshwater lakes are largely determined by regional climate-controlled temperatures and the maximum density of water ( $1 \text{ g/cm}^3$ ) at  $3.98^\circ\text{C}$  (Hutchinson and Löffler, 1956). For example, if autumn cooling lowers surface waters to  $\sim 4^\circ\text{C}$ , then a density inversion is established which produces downward displacement of denser water and mixing of the water column. During summer, warming and expansion of surface water creates vertical density stratification where the densest water remains at  $\sim 4^\circ\text{C}$  at the bottom of the lake. Generally, deep, non-tropical, freshwater lakes maintain  $4^\circ\text{C}$  bottom water temperatures year-round (Butcher et al., 2015), and are therefore insensitive to mean annual air temperatures (MAAT).

Unlike freshwater lakes, the behavior of saline lakes is not constrained by the  $\sim 4^\circ\text{C}$  density maximum of water, as brine densities are considerably higher due to the dissolved salt. Furthermore, the change in density with temperature of saline lakes is much higher than their freshwater counterparts, which contributes to their increased stability (Ferris and Burton, 1988). Saline lakes in non-tropical climates may therefore behave like freshwater tropical lakes, where thermal structures and bottom water temperatures reflect seasonal and annual air temperatures. Nevertheless, the general relationship between saline lake floor temperatures and climate is poorly established, and thus interpretations of temperature data from fluid inclusions in halite precipitated on the floor of ancient Searles Lake first requires investigation of modern saline lakes.

The Great Salt Lake region experienced abnormally high precipitation from 1982–1984, which, combined with large snowpack during the winter of 1985, produced a 3.72 m rise of lake level by 1987 to the historical record of 1283.77 m (Fig. 3A) (Stephens, 1990). Increased freshwater inflow to Great Salt Lake retarded annual overturn (holomixis) and maintained stable meromixis (permanent stratification) until lake level dropped in the 1990s (Fig. 3B). As the depth of Great Salt Lake increased (Fig. 3B), the range of bottom water temperatures narrowed and converged on the mean annual air temperature (Fig. 3C), showing that 1) the annual range of bottom water temperatures is anti-correlated to lake depth (Fig. 3D) and 2) the average bottom water temperature is climatically significant as it reflects MAAT. For Great Salt Lake, bottom water temperature is constant and equal to MAAT of  $\sim 10^\circ\text{C}$  when lake depths are  $\geq 12 \text{ m}$  (Fig. 3E).

Data for nine non-tropical saline lakes of various depths and salinities confirm the Great Salt Lake observations, as they show a strong correlation ( $r = 0.97$ ) between mean annual air temperatures and average bottom water temperatures, including shallow ( $< 10 \text{ m}$ -deep) saline lakes (Fig. 4A). This correlation means that even if bottom water temperatures are not constant, they still oscillate seasonally around mean annual air temperatures and support the interpretation that layer-averaged Brillouin temperatures from Searles Lake halites record MAAT.

A consistent relationship exists between lake depth and bottom water temperature range for all saline lakes (Fig. 4B). The range of bottom water temperatures decreases with depth to  $\sim 12\text{--}22 \text{ m}$  and remains relatively constant ( $< 2^\circ\text{C}$  variability) at greater depths. This lake depth-temperature relationship is likely due to the combined effects of limited light penetration, wave base, and density stratification and as such is expected to vary between lakes. Here, the linear regression in Fig. 4B is used for an upper estimate of Searles Lake depths, and the relationship for Great Salt Lake (Fig. 3E) is used for a lower estimate. Based on the range of temperatures determined within individual halite layers, calculated paleo-depths for Pleistocene/Holocene Searles Lake during

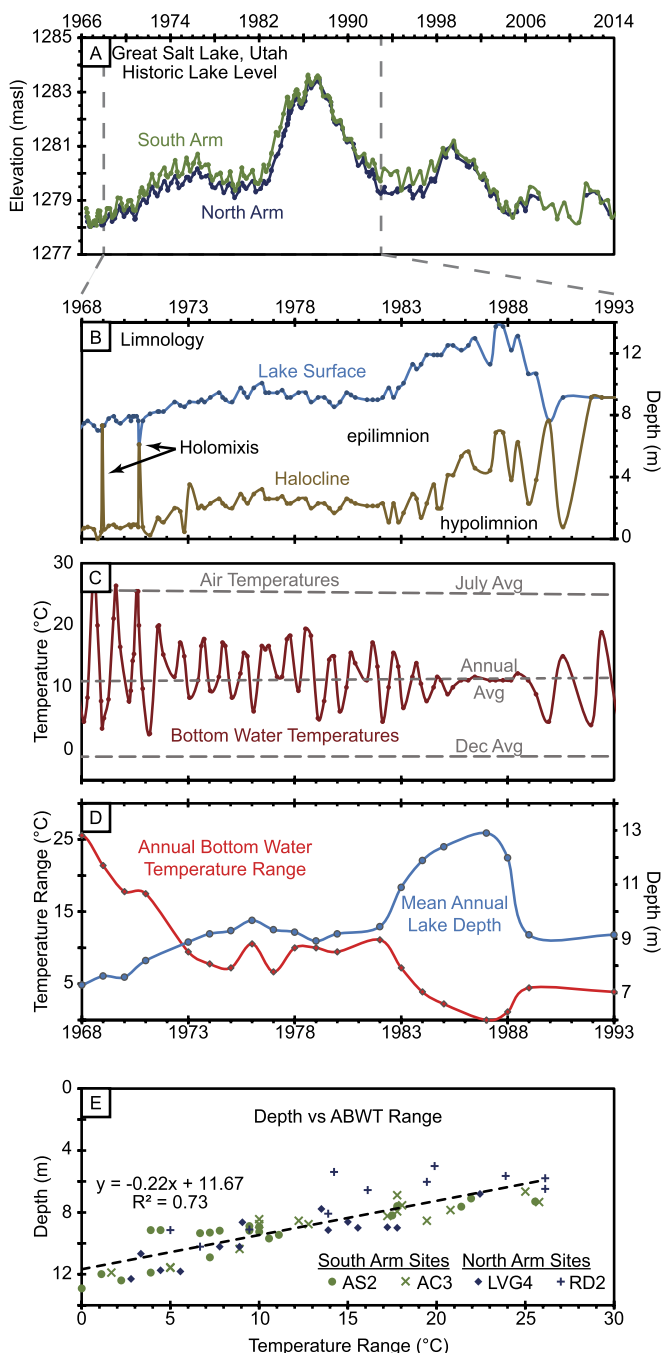


**Fig. 3.** Elevation, depth and temperature from Great Salt Lake, Utah. Data collected and maintained by the Utah Department of Natural Resources, Utah Geological Survey (see Rupke and McDonald, 2012). (A) Historic lake elevation of Great Salt Lake; note the abrupt lake level rise starting in 1982. (B) Lake level and stratification. (C) Comparison of air temperatures with bottom water temperatures. (D) Inverse relationship between mean annual bottom water temperature range and mean annual lake depth. (E) Mean annual lake depth plotted against bottom water temperature range. Data in (B)–(D) are from site AS2. See Fig. S6 for GSL sample locations.

times of halite precipitation ranged from 10.1 to 22.0 m (Table 1). The range of paleodepths captures the range of empirical data for modern saline lakes. Brillouin measurements for Searles Lake halite units provide a *minimum* annual bottom water temperature range, and therefore a *maximum* lake depth estimate. Additionally, the deeper (22.0 m) estimates are derived from modern lakes with low salinity (relative to Great Salt Lake) and are likely less stable (greater bottom water temperature variability) than if they were

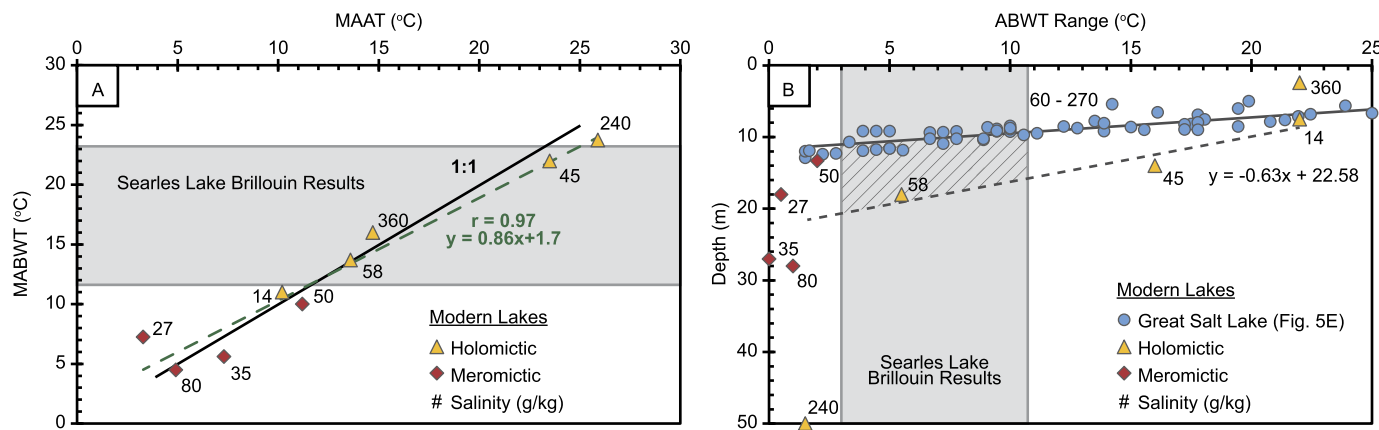


**Fig. 4.** Climate-lake relationships for non-tropic saline lakes. (A) Mean annual air temperature (MAAT) versus mean annual bottom water temperature (MABWT) and (B) Annual bottom water temperature (ABWT) range versus lake depth. Data point labels are salinity in g/L. Data listed in Appendix A.

halite-saturated. For these reasons, the shallower depth estimates of  $\sim 10$  m are more likely representative of a halite-saturated Searles Lake. Smith (2009) used basin hypsometry and stratigraphic masses to calculate a 0–12 m depth for a halite saturated Searles Lake. Our findings therefore overlap with previous estimates but suggest that the deeper of Smith's (2009) 0–12 m estimate is more likely. A deeper, perennial Searles Lake was also argued by Olson and Lowenstein (2021) as necessary to account for long-term ion inheritance and Searles Lake mass-balance.

#### 4.2. Brillouin/brGDGT versus thermodynamic models

A comparison of Brillouin and brGDGT temperature reconstructions from the Searles Lake core from 40–5 m is shown in Fig. 5C. For the most part, interlayered salts (fluid inclusions) and muds (brGDGTs) record similar temperatures, within the uncertainties of each proxy. Both proxies also record similar temperature ranges and temporal trends: the average reconstructed temperature is  $17.5 \pm 4.1$  °C for Brillouin and  $18.7 \pm 2.8$  °C for brGDGTs, with temperature ranges of  $10.6 \pm 6.8$  °C for Brillouin and  $10.5 \pm 5.8$  °C for brGDGTs. For the Holocene, average reconstructed temperatures are  $21.1 \pm 2.1$  °C from Brillouin and  $19.8 \pm 2.2$  °C from brGDGTs, similar to the modern mean annual temperature at Searles Lake, of 20.1 °C.

A temperature record for Searles Lake can also be reconstructed from the assemblages and sequences of evaporite minerals (Olson and Lowenstein, 2021). Trona and burkeite, for instance, are thermodynamically stable only at temperatures above 15 °C, below which natron and mirabilite precipitate (Fig. 2). The common occurrence of trona and burkeite in the Lower Salt and Upper Salt (Fig. 5B), and the lack of natron and mirabilite, thus implies brine temperatures  $\geq 15$  °C during evaporite deposition. An upper limit for brine temperature (29 °C) is also constrained by evaporite minerals. Above 29 °C, burkeite precipitates prior to trona, but this sequence is never observed in the Searles Lake deposit. While the temperature thresholds are highly dependent on brine chemistry and  $p\text{CO}_2$ , both are well constrained by the evaporite record (Supplementary Material).

For the Upper Salt (15.6–0 ka), Brillouin and brGDGT temperatures are consistent with the 15–29 °C temperature estimates from the phase assemblages and sequences, and the three temperature proxies are in good agreement. However, Brillouin temperatures for the S4 unit of the Lower Salt are  $11.8 \pm 3.6$  °C, indicating that the Na-carbonate and Na-sulfate phases within that unit should consist of natron and mirabilite instead of trona and burkeite (Fig. 2). Brillouin and brGDGT temperatures below 15 °C occur in other

intervals of the Lower Salt (38.5–22.6 ka) (e.g., M2–5; S7), indicating natron and mirabilite should also occur in these units. In contrast, the Na-carbonates and Na-sulfates of the Lower Salt are chiefly composed of trona and burkeite, which form above 15 °C. Based on these observations, salts formed in the warm season are preferentially preserved in the Searles Lake deposit. We conclude that the preservation of evaporite deposits is sensitive to seasonal changes in brine temperature, especially low temperature salts such as mirabilite and natron, which form at the lake surface in winter but commonly dissolve in warmer bottom waters.

#### 4.3. Temperature record of Searles Lake

Here, Searles Lake Brillouin and brGDGT temperatures are combined into a 45 kyr paleotemperature record (Table 2) and compared to other regional temperature records. During the last glacial (45–14 ka), Searles Lake was perennial (i.e., never desiccated) and experienced dramatic hydrologic variability as indicated by alternating deposition of salts and muds. Searles Lake temperatures during the last glacial were  $\sim 2.2$  °C lower than today ( $17.9 \pm 3.1$  °C) but highly variable, with temperatures ranging from 8.3 °C below to 3.8 °C above mean annual air temperature (MAAT) (Table 2). During the Last Glacial Maximum (LGM- 23–19 ka), Searles was 2.0 °C lower than today which was followed by deglacial warming of 2.0 °C from 19 ka to 11 ka. Holocene (11–0 ka) temperatures of Searles Lake (20.2 °C) are indistinguishable from modern values (20.1 °C) and exhibit greater stability – fluctuating by only  $-2.1$  °C to  $+2.8$  °C relative to MAAT. The Holocene has been as a prolonged dry period at Searles, with low lake levels and extensive evaporite deposition.

At glacial/interglacial timescales, the Searles Lake temperature proxies agree with regional archives, recording colder/wetter conditions during the last glacial (45–14 ka), temperatures rising to modern values during the deglacial (19–11 ka), and warm/dry conditions during the Holocene. Regional groundwater temperatures during the last glacial were  $6.2 \pm 0.6$  °C lower than today in the San Diego area and  $4.2 \pm 1.1$  °C below modern in the Mojave Desert (Fig. 6B) (Kulogoski et al., 2009; Seltzer et al., 2019). During the LGM, SST along the California margin was  $\sim 4$  °C cooler than today (Herbert et al., 2001). In the Sierra Nevada, the Tioga Glaciation (27–15 ka) reached a maximum snowline depression (ELA) of 1200 m (Phillips, 2017), which corresponds to  $\sim 5$ –6 °C lower MAAT than today (Plummer, 2002). The effects of advancing and retreating Sierra Nevada glaciers are observed in nearby lake records by variations in pollen. Juniper pollen from Owens

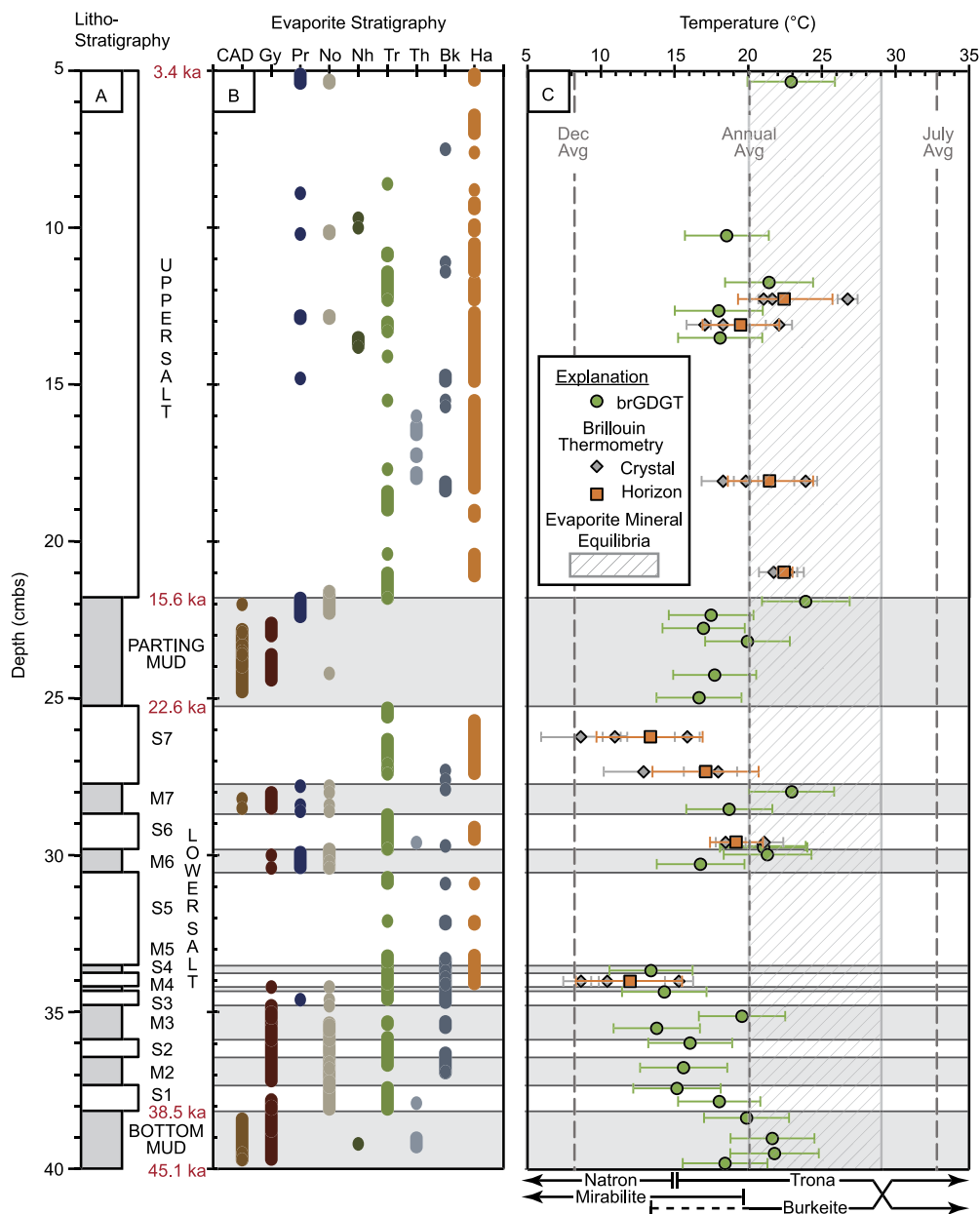


**Fig. 5.** Comparison of Seales Lake temperature proxies. (A) Lithostratigraphy, (B) Evaporite mineral stratigraphy, and (C) Brillouin and brGDGT temperatures from Seales Lake core SLAPP-SRLS17-1A/B. Modeled evaporite facies temperature range (20–29 °C) of Olson and Lowenstein (2021) shown with diagonal lines. Temperature thresholds (bottom arrows) from Fig. 2. Note the lack of natron and/or mirabilite in the evaporite stratigraphy. CAD = Calcite/Aragonite/Dolomite, Gy = Gaylussite, Pr = Pirssonite, No = Northupite, Nh = Nahcolite, Tr = Trona, Th = Thenardite, Bk = Burkeite, Ha = Halite, cmbs = composite meters below surface.

**Table 2**  
Summary of Seales Lake Paleotemperatures.

Interval	Age (kya)	n	Mean <sup>†</sup>	Temperature (°C)*		Range
				Min. <sup>#</sup>	Max. <sup>#</sup>	
Holocene	12-0	7	20.2 ± 2.1	18.0 ± 3.0	22.9 ± 3.0	4.9 ± 6.0
Last Glacial	45-14	28	17.9 ± 3.1	<b>11.8 ± 3.6</b>	23.9 ± 3.0	12.1 ± 6.6
MIS 1	14-0	9	20.4 ± 2.0	18.0 ± 3.0	22.9 ± 3.0	4.9 ± 6.0
MIS 2	29-14	15	18.8 ± 2.8	<b>13.2 ± 3.6</b>	23.9 ± 3.0	10.7 ± 6.6
MIS 3	45-29	13	16.8 ± 3.2	<b>11.8 ± 3.6</b>	21.8 ± 3.0	10.0 ± 6.6
Deglaciation	19-11	5	20.1 ± 3.1	17.0 ± 2.8	23.9 ± 3.0	6.9 ± 5.8
LGM	23-19	3	18.1 ± 1.7	16.7 ± 2.9	19.9 ± 2.9	3.3 ± 5.8
SLAPP-SRLS17	45-0	37	18.4 ± 3.1	<b>11.8 ± 3.6</b>	23.9 ± 3.0	12.1 ± 6.6

\*  $1\sigma$  uncertainties.

† Weighted mean  $\pm$  unbiased weighted SD.

# **Bold** values indicate Brillouin (salt) temperatures.

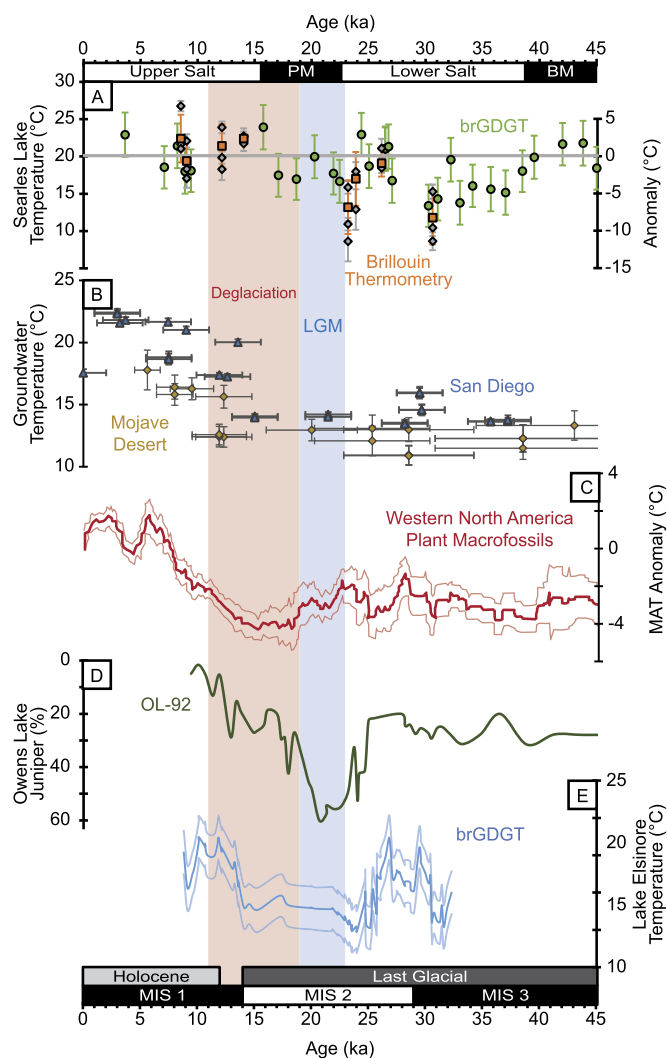


**Fig. 6.** Comparison of regional temperature records. (A) Seares Lake temperatures from Brillouin thermometry and brGDGTs. (B) Groundwater noble gas temperatures from the Mojave Desert (Kulogoski et al., 2009) and San Diego area (Seltzer et al., 2019). (C) Mean annual temperature anomaly ( $\pm 2$  SE) estimated by CRACKLE using plant macrofossil (packrat) communities (Harbert and Nixon, 2018). (D) Juniper pollen from Owens Lake core OL-92 (Woolfenden, 2003). (E) Temperature record ( $\pm 2\sigma$ ) from Lake Elsinore, California (Peakins et al., 2019). Blue shading highlights the LGM (23–19 ka) and red shading highlight deglaciation (19–11 ka). See Fig. S6 for locations of records discussed. (For interpretation of the colors in the figure(s), the reader is referred to the web version of this article.)

Lake core OL-92, for example, indicates a 500–600 m downslope expansion of pinyon-juniper woodland as glaciers advanced and temperatures decreased between 25 ka and 20 ka (LGM). This was followed by a sharp decline in Juniper pollen during deglaciation (19–11 ka; Fig. 6D) (Woolfenden, 2003). A regional hydroclimate record for the western United States was computed from a large dataset of plant macrofossils (packrat middens) (Fig. 6C) (Harbert and Nixon, 2018). A perfect correlation is not expected given the large geographical area (Supplementary Material). But the macrofossil temperature trend during the last glacial is in general agreement with Seares Lake temperatures, including consistently low mean annual temperatures (MATs) during the last glacial, 45–15 ka, warming trend during deglaciation, and maximum MATs in the Holocene (Fig. 6C).

At millennial timescales, Seares Lake sediments record large swings in terrestrial temperatures during the last glacial (45–14 ka), with Brillouin and brGDGTs indicating variability of 12.1 °C. Comparable millennial-scale variability is seen in Lake Elsinore

where the pre-LGM (33–23 ka) brGDGT record shows variability of 12.6 °C (Fig. 6E) (Peakins et al., 2019). Seares Lake temperatures vary by 11.1 °C during the same period (Fig. 6A). In contrast, California margin SSTs fluctuated by only 1.1 °C from 33–23 ka (Herbert et al., 2001) and regional groundwaters varied by only 2.5 °C (Fig. 6B) (Kulogoski et al., 2009; Seltzer et al., 2019). This comparison corroborates that large thermal reservoirs, such as groundwater and the ocean, do not respond to millennial scale climate change with the same sensitivity as lakes. During the Holocene, temperature ranges narrow to 4.9 °C for Seares Lake and 6.9 °C for Lake Elsinore.

## 5. Conclusions

- Brillouin thermometry on fluid inclusions in halite yields temperatures of bottom brines during periods of evaporite deposition in Seares Lake, California, from 45–0 ka.
- The reconstruction of temperatures using the brGDGT thermometer from mud samples reflects mean months above freezing, and corroborates the Brillouin reconstructions of temperature.
- The two techniques measure different materials and facies, which provides a reconstruction of temperature across changing depositional environments in Pleistocene Seares Lake.
- Brillouin thermometry yields a record of bottom water conditions. The mean annual bottom water temperature (MABWT) of non-tropical saline lakes is a proxy for mean annual air temperature (MAAT), whereas the annual range in bottom water temperatures is a proxy for lake depth. For salt saturated lakes, this allows reconstruction of temperature records during lake low-stands, an important compliment to more common high-stand records.
- Between 45 ka to 2.8 ka, when Seares Lake was at halite saturation, the brine was ~10 m deep. Such depths produce two temperature regimes: variable surface temperatures and near-constant bottom brine temperatures. In saline-alkaline lakes, low temperature- salts may precipitate in cold surface waters and then settle to warmer bottom waters where they dissolve, resulting in a temperature-biased evaporite record. Paleotemperature reconstructions based on evaporite phase equilibria should therefore be evaluated with independent proxies such as Brillouin thermometry or brGDGTs.
- This study introduces a paired proxy approach to study temperature across changing facies in perennial lakes with evaporite-mud alterations. The two proxies incorporate low and high salinity facies to reconstruct temperatures and hydroclimate. The new Seares Lake temperature reconstructions indicate colder conditions during the last glacial, deglacial warming to modern temperatures, and warm conditions during the Holocene. At millennial timescales, Seares Lake dual proxy reconstruction indicates significant temperature variability during the last glacial, with temperatures ranging from 8.3 °C lower than modern to 3.8 °C higher.

## CRediT authorship contribution statement

**Kristian J. Olson:** Conceptualization, Funding acquisition, Investigation, Methodology, Visualization, Writing – original draft. **Emmanuel Guillerm:** Conceptualization, Formal analysis, Investigation, Methodology, Supervision, Writing – review & editing. **Mark D. Peaple:** Conceptualization, Formal analysis, Investigation, Methodology, Writing – review & editing. **Tim K. Lowenstein:** Conceptualization, Funding acquisition, Supervision, Writing – original draft. **Véronique Gardien:** Conceptualization, Funding acquisition, Resources, Supervision, Writing – review & editing. **Frédéric**

**Caupin:** Conceptualization, Funding acquisition, Resources, Supervision, Writing – review & editing. **Sarah J. Feakins:** Conceptualization, Funding acquisition, Resources, Supervision, Writing – review & editing. **Jessica E. Tierney:** Funding acquisition, Resources, Supervision, Writing – review & editing. **Justin Stroup:** Conceptualization, Investigation, Methodology. **Steve Lund:** Resources. **David McGee:** Conceptualization, Funding acquisition, Resources, Supervision, Writing – review & editing.

## Declaration of competing interest

The authors declare that they have no known competing financial interests or personal relationships that could have appeared to influence the work reported in this paper.

## Data availability

The data associated with this article are archived at the NOAA paleoclimate database. <https://www.nci.noaa.gov/access/paleo-search/study/36836>

## Acknowledgements

We thank Jade Brush and Searles Valley Minerals Inc. for access and support during recovery of core SLAPP-SRLS17. Sample material used in this project was provided by the Continental Scientific Drilling (CSD) Facility, University of Minnesota. This material is based upon research supported by the Chateaubriand Fellowship of the Office for Science & Technology of the Embassy of France in the United States to KO, the Comer Family Foundation funding to TL and DM, US National Science Foundation Award NSF-EAR-1903659, 1903665, 1903519, and 1903544 respectively to TL, SF, JS, and DM, with additional support from GSA, AAPG, and SEG graduate student grants to KO. Part of this work was performed within the framework of the EUR H2O'Lyon (ANR-17-EURE-0018) of Université de Lyon (UdL), within the program “Investissements d’Avenir” operated by the French National Research Agency (ANR). We thank Patrick Murphy for assistance with GDGT analyses at U. Arizona, supported by Packard Foundation funding to JT.

## Appendix A. Supplementary material

Supplementary material related to this article can be found online at <https://doi.org/10.1016/j.epsl.2022.117913>.

## References

Bacon, S.N., Jayko, A.S., Owen, L.A., Lindvall, S.C., Rhodes, E.J., Schumer, R.A., Decker, D.L., 2020. A 50,000-year record of lake-level variations and overflow from Owens Lake, eastern California, USA. *Quat. Sci. Rev.* 238, 106312. <https://doi.org/10.1016/j.quascirev.2020.106312>.

Benson, L., 1999. Records of millennial-scale climate change from the Great Basin of the Western United States. In: Clark, U., Webb, S., Keigwin, D. (Eds.), *Geophysical Monograph Series*. American Geophysical Union, Washington, D. C., pp. 203–225.

Benson, L., Lund, S., Negrini, R., Linsley, B., Zic, M., 2003. Response of North American Great Basin lakes to Dansgaard–Oeschger oscillations. *Quat. Sci. Rev.* 22, 2239–2251. [https://doi.org/10.1016/S0277-3791\(03\)00210-5](https://doi.org/10.1016/S0277-3791(03)00210-5).

Bischoff, J.L., Rosenbauer, R.J., Smith, G.I., 1985. Uranium-series dating of sediments from Searles Lake: differences between continental and marine climate records. *Science*, 1222–1224. <https://doi.org/10.1126/science.227.4691.1222>.

Brall, N.S., Gardien, V., Ariztegui, D., Sorrel, P., Guillerm, E., Caupin, F., 2022. Reconstructing lake bottom water temperatures and their seasonal variability in the Dead Sea Basin during MIS5e. *Depositional Record*. Accepted Author Manuscript. <https://doi.org/10.1002/dep.2185>.

Butcher, J.B., Nover, D., Johnson, T.E., Clark, C.M., 2015. Sensitivity of lake thermal and mixing dynamics to climate change. *Clim. Change* 129, 295–305. <https://doi.org/10.1007/s10584-015-1326-1>.

Cook, B.I., Mankin, J.S., Williams, A.P., Marvel, K.D., Smerdon, J.E., Liu, H., 2021. Uncertainties, limits, and benefits of climate change mitigation for soil moisture drought in southwestern North America. *Earth’s Future* 9, e2021EF002014. <https://doi.org/10.1029/2021EF002014>.

De Jonge, C., Hopmans, E.C., Zell, C.I., Kim, J.H., Schouten, S., Sinninghe Damsté, J.S., 2014. Occurrence and abundance of 6-methyl branched glycerol dialkyl glycerol tetraethers in soils: implications for palaeoclimate reconstruction. *Geochim. Cosmochim. Acta* 141, 97–112. <https://doi.org/10.1016/j.gca.2014.06.013>.

El Mekki-Azouzi, M.E., Tripathi, C.S.P., Pallares, G., Gardien, V., Caupin, F., 2015. Brillouin spectroscopy of fluid inclusions proposed as a paleothermometer for subsurface rocks. *Sci. Rep.* 5, 9. <https://doi.org/10.1038/srep13168>.

Feakins, S.J., Wu, M.S., Ponton, C., Tierney, J.E., 2019. Biomarkers reveal abrupt switches in hydroclimate during the last glacial in southern California. *Earth Planet. Sci. Lett.* 515, 164–172. <https://doi.org/10.1016/j.epsl.2019.03.024>.

Ferris, J.M., Burton, H.R., 1988. The annual cycle of heat content and mechanical stability of hypersaline Deep Lake, Vestfold Hills, Antarctica. *Hydrobiologia* 165, 115–128. <https://doi.org/10.1007/BF00025579>.

Gale, H.S., 1914. Salines in the Owens, Searles, and Panamint basins, southeastern California, U.S. Geol. Surv. Bull. 580-L, 251–323. <https://doi.org/10.3133/b580L>.

Guillerm, E., 2019. Turning halite fluid inclusions into accurate paleothermometers with Brillouin spectroscopy. Ph.D. thesis. Université Claude Bernard Lyon 1, Lyon, France, p. 229. <https://www.theses.fr/2019LYSE1284>.

Guillerm, E., Gardien, V., Ariztegui, D., Caupin, F., 2020. Restoring halite fluid inclusions as an accurate paleothermometer: Brillouin thermometry versus microthermometry. *Geostand. Geoanal. Res.* 44, 243–264. <https://doi.org/10.1111/ggr.12312>.

Harbert, R.S., Nixon, K.C., 2018. Quantitative late quaternary climate reconstruction from plant macrofossil communities in western North America. *Open Quat.* 4, 1–13. <https://doi.org/10.5334/oq.46>.

Herbert, T.D., Schuffert, J.D., Andreassen, D., Heusser, L., Lyle, M., Mix, A., Ravelo, A.C., Stott, L.D., Herguera, J.C., 2001. Collapse of the California current during glacial maxima linked to climate change on land. *Science* 293, 71–76. <https://doi.org/10.1126/science.1059209>.

Hopmans, E.C., Schouten, S., Sinninghe Damsté, J.S., 2016. The effect of improved chromatography on GDGT-based palaeoproxies. *Org. Geochem.* 93, 1–6. <https://doi.org/10.1016/j.orggeochem.2015.12.006>.

Hutchinson, G.E., Löffler, H., 1956. The thermal classification of lakes. In: *Proceedings of the National Academy of Sciences of the United States of America*, vol. 42, p. 84.

Ibarra, D.E., Oster, J.L., Winnick, M.J., Caves Rugenstein, J.K., Byrne, M.P., Chamberlain, C.P., 2018. Warm and cold wet states in the western United States during the Pliocene–Pleistocene. *Geology* 46, 355–358. <https://doi.org/10.1130/G39962.1>.

Kulongsoski, J.T., Hilton, D.R., Izbicki, J.A., Belitz, K., 2009. Evidence for prolonged El Niño-like conditions in the Pacific during the Late Pleistocene: a 43 ka noble gas record from California groundwaters. *Quat. Sci. Rev.* 28, 2465–2473. <https://doi.org/10.1016/j.quascirev.2009.05.008>.

Lensky, N.G., Dvorkin, Y., Lyakhovsky, V., Gertman, I., Gavrieli, I., 2005. Water, salt, and energy balances of the Dead Sea. *Water Resour. Res.* 41, W12418. <https://doi.org/10.1029/2005WR004084>.

Lin, J.C., Broecker, W.S., Hemming, S.R., 1998. A reassessment of U-Th and  $^{14}\text{C}$  ages for lat-glacial high-frequency hydrological events at Searles Lake, California. *Quat. Res.* 49, 11–23. <https://doi.org/10.1006/qres.1997.1949>.

Lowenstein, T.K., Li, J., Brown, C., 1998. Paleotemperatures from fluid inclusions in halite: method verification and a 100,000 year paleotemperature record, Death Valley, CA. *Chem. Geol.* 150, 223–245. [https://doi.org/10.1016/S0009-2541\(98\)00061-8](https://doi.org/10.1016/S0009-2541(98)00061-8).

Lowenstein, T.K., Li, J., Brown, C., Roberts, S.M., Ku, T.-L., Luo, S., Yang, W., 1999. 200 ky paleoclimate record from Death Valley salt core. *Geology* 27, 3–6. [https://doi.org/10.1130/0091-7613\(1999\)027%3C0003:KYPRFD%3E2.3;2](https://doi.org/10.1130/0091-7613(1999)027%3C0003:KYPRFD%3E2.3;2).

Lund, S., Benson, L., Negrini, R., 2021. Timing of Sierra Nevada stadial/interstadial variations from 15 to 56 ka. *Quat. Int.* 583, 31–38. <https://doi.org/10.1016/j.quaint.2021.02.007>.

Martínez-Sosa, P., Tierney, J.E., Stefanescu, I.C., Dearing Crampton-Flood, E., Shuman, B.N., Routson, C., 2021. A global Bayesian temperature calibration for lacustrine brGDGTs. *Geochim. Cosmochim. Acta* 305, 87–105. <https://doi.org/10.1016/j.gca.2021.04.038>.

Olson, K.J., Lowenstein, T.K., 2021. Searles lake evaporite sequences: indicators of late Pleistocene/Holocene lake temperatures, brine evolution, and  $\text{pCO}_2$ . *Geol. Soc. Am. Bull.* <https://doi.org/10.1130/B35857.1>.

Peaple, M.D., Bhattacharya, T., Lowenstein, T., McGee, D., Olson, K., Stroup, J.S., Tierney, J.E., Feakins, S.J., 2022. Biomarker and pollen evidence for late Pleistocene pluvials in the Mojave Desert. *Earth Space Sci. Open Arch.* 45. <https://doi.org/10.1002/essoar.1051122.1>.

Phillips, F., 2017. Glacial chronology of the Sierra Nevada, California, from the last glacial maximum to the Holocene. *Cuad. Invest. Geogr.* 43, 527. <https://doi.org/10.18172/cig.3233>.

Phillips, F.M., Campbell, A.R., Smith, G.I., Bischoff, J.L., 1994. Interstadial climatic cycles: a link between western North America and Greenland? *Geology* 22, 1115–1118. [https://doi.org/10.1130/0091-7613\(1994\)022<1115:ICCALB>2.3.CO;2](https://doi.org/10.1130/0091-7613(1994)022<1115:ICCALB>2.3.CO;2).

Pierce, D.W., Cayan, D.R., Das, T., Maurer, E.P., Miller, N.L., Bao, Y., Kanamitsu, M., Yoshimura, K., Snyder, M.A., Sloan, L.C., Franco, G., 2013. The key role of heavy precipitation events in climate model disagreements of future annual precipitation changes in California. *J. Climate* 26, 5879–5896. <https://doi.org/10.1175/JCLI-D-12-00766.1>.

Plummer, M.A., 2002. Paleoclimatic conditions during the Last Deglaciation inferred from combined analysis of pluvial and glacial records. Ph.D. thesis. New Mexico Institute of Mining and Technology, Socorro, New Mexico, p. 308. [https://www.nmt.edu/academics/ees/theses/theses\\_1936-2014/2002d\\_plummer\\_ma.pdf](https://www.nmt.edu/academics/ees/theses/theses_1936-2014/2002d_plummer_ma.pdf).

Pretti, V.A., Stewart, B.W., 2002. Solute sources and chemical weathering in the Owens Lake watershed, eastern California: solute sources and chemical weathering. *Water Resour. Res.* 38, 2–1–2–18. <https://doi.org/10.1029/2001WR000370>.

Quirk, B.J., Moore, J.R., Laabs, B.J., Caffee, M.W., Plummer, M.A., 2018. Termination II, last glacial maximum, and lateglacial chronologies and paleoclimate from Big Cottonwood Canyon, Wasatch Mountains, Utah. *Geol. Soc. Am. Bull.* 130, 1889–1902. <https://doi.org/10.1130/B31967.1>.

Reheis, M.C., Adams, K.D., Oviatt, C.G., Bacon, S.N., 2014. Pluvial lakes in the Great Basin of the western United States—a view from the outcrop. *Quat. Sci. Rev.* 97, 33–57. <https://doi.org/10.1016/j.quascirev.2014.04.012>.

Reheis, M.C., Miller, D.M., McGeehin, J.P., Redwine, J.R., Oviatt, C.G., Bright, J., 2015. Directly dated MIS 3 lake-level record from Lake Manix, Mojave Desert, California, USA. *Quat. Res.* 83, 187–203. <https://doi.org/10.1016/j.yqres.2014.11.003>.

Roberts, S.M., Spencer, R.J., 1995. Paleotemperatures preserved in fluid inclusions in halite. *Geochim. Cosmochim. Acta* 59, 3929–3942. [https://doi.org/10.1016/0016-7037\(95\)00253-V](https://doi.org/10.1016/0016-7037(95)00253-V).

Rupke, A.L., McDonald, A., 2012. Great Salt Lake brine chemistry database, 1966–2011. In: Utah Geological Survey, vol. 596, Salt Lake City, UT, pp. 1–7. [https://ugspub.nr.utah.gov/publications/open\\_file\\_reports/ofr-596/ofr-596.pdf](https://ugspub.nr.utah.gov/publications/open_file_reports/ofr-596/ofr-596.pdf).

Santi, L.M., Arnold, A.J., Ibarra, D.E., Whicker, C.A., Mering, J.A., Lomarda, R.B., Lora, J.M., Tripati, A., 2020. Clumped isotope constraints on changes in latest Pleistocene hydroclimate in the northwestern Great Basin: Lake Surprise, California. *Geol. Soc. Am. Bull.* 132, 2669–2683. <https://doi.org/10.1130/B35484.1>.

Seager, R., Ting, M., Held, I., Kushnir, Y., Lu, J., Vecchi, G., Huang, H.P., Harnik, N., Leetmaa, A., Lau, N.C., Li, C., 2007. Model projections of an imminent transition to a more arid climate in southwestern North America. *Science* 316, 1181–1184. <https://doi.org/10.1126/science.1139601>.

Seager, R., Tzanova, A., Nakamura, J., 2009. Drought in the southeastern United States: causes, variability over the last millennium, and the potential for future hydroclimate change. *J. Climate* 22, 5021–5045. <https://doi.org/10.1175/2009JCLI2683.1>.

Seltzer, A.M., Ng, J., Danskin, W.R., Kulongoski, J.T., Gannon, R.S., Stute, M., Severinghaus, J.P., 2019. Deglacial water-table decline in Southern California recorded by noble gas isotopes. *Nat. Commun.* 10, 5739. <https://doi.org/10.1038/s41467-019-13693-2>.

Sirota, I., Enzel, Y., Lensky, N.G., 2017. Temperature seasonality control on modern halite layers in the Dead Sea: in situ observations. *Geol. Soc. Am. Bull.* 129, 1181–1194. <https://doi.org/10.1130/B31661.1>.

Smith, G.I., 1979. Subsurface stratigraphy and geochemistry of late Quaternary evaporites, Searles Lake, California. U.S. Geological Survey Professional Paper, vol. 1043, p. 130.

Smith, G.I., 2009. Late Cenozoic geology and lacustrine history of Searles Valley, Inyo and San Bernardino Counties, California. U.S. Geol. Surv. Prof. Pap. 128. <https://pubs.usgs.gov/pp/1727/>.

Smoot, J.P., Lowenstein, T.K., 1991. Chapter 3 depositional environments of non-marine evaporites. In: Melvin, J.L. (Ed.), *Developments in Sedimentology*, vol. 50. Elsevier, pp. 189–347.

Stephens, D.W., 1990. Changes in lake levels, salinity and the biological community of Great Salt Lake (Utah, USA), 1847–1987. *Hydrobiologia* 197, 139–146. <https://doi.org/10.1007/BF00026946>.

Stroup, J.S., Olson, K., Lowenstein, T.K., Jost, A.B., Mosher, H.M., Peaple, M.D., Feakins, S.J., Chen, C.Y., Lund, S.P., McGee, D., 2022. A >200 ka U-Th based chronology from lacustrine evaporites, Searles Lake, CA. *Earth Space Sci. Open Arch.* 42. <https://doi.org/10.1002/essoar.10512405.1>.

Wang, H., Liu, W., He, Y., Zhou, A., Zhao, H., Liu, H., Cao, Y., Hu, J., Meng, B., Jiang, J., Kolpakova, M., Krivonogov, S., Liu, Z., 2021. Salinity-controlled isomerization of lacustrine brGDGTs impacts the associated MBT<sup>573E</sup> terrestrial temperature index. *Geochim. Cosmochim. Acta* 305, 33–48. <https://doi.org/10.1016/j.gca.2021.05.004>.

Woolfenden, W.B., 2003. A 180,000-year pollen record from Owens Lake, CA: terrestrial vegetation change on orbital scales. *Quat. Res.* 59, 430–444. [https://doi.org/10.1016/S0033-5894\(03\)00033-4](https://doi.org/10.1016/S0033-5894(03)00033-4).